Controlling Hydrogen Evolution during Photoreduction of CO 2 to Formic Acid Using [Rh(R-bpy)(Cp*)Cl] + Catalysts: A Structure–Activity Study

Tanya K Todorova, Tran Ngoc Huan, Xia Wang, Hemlata Agarwala, Marc Fontecave

Controlling Hydrogen Evolution during CO_2 Photoreduction to Formic Acid using $[Rh(R\text{-}bpy)(Cp^*)Cl]^+$ Catalysts: A Structure-Activity Study.

Tanya K. Todorova, Tran Ngoc Huan, Xia Wang, Hemlata Agarwala, Marc Fontecave*

Laboratoire de Chimie des Processus Biologiques, UMR 8229 CNRS, Collège de France, Université Paris 6, 11 Place Marcelin Berthelot, 75231 Paris Cedex 05, France

ABSTRACT: The photochemical CO_2 reduction to formic acid catalyzed by a series of $[Rh(4,4'\text{-}R\text{-}bpy)(Cp^*)Cl]^+$ and $[Rh(5,5'\text{-}COOH\text{-}bpy)(Cp^*)Cl]^+$ complexes (Cp^* = pentamethylcyclopentadienyl, bpy = 2,2′-bipyridine, R = OCH_3, CH_3, H, $COOC_2H_5$, CF_3, NH_2 and COOH) was studied in order to assess how modifications in the electronic structure of the catalyst affect its selectivity, defined as the HCOOH : H_2 product ratio. A direct molecular-level influence of the functional group on the initial reaction rate for CO_2 *vs*. proton reduction reactions was established. Density functional theory computations elucidated for the first time the respective role of the [RhH] *vs* [Cp*H] tautomers, recognizing the rhodium hydride as the key player for both reactions. In particular, our calculations explain the observed tendency of electron-donating substituents to favor CO_2 reduction by means of lowering the hydricity of the Rh–H bond, resulting in lower hydride transfer barrier towards formic acid production as compared to substituents with electron-withdrawing nature that favor more strongly the proton reduction to hydrogen.

INTRODUCTION

The reduction of carbon dioxide is one of the most promising approaches to valorize CO_2 into fuels or chemicals.[1–5] However, the chemical inertness of CO_2 makes its reduction a very challenging task, requiring the use of catalysts in order to increase the rate, efficiency and selectivity of the chemical transformations involved.[2,6–10] Molecular catalysts have attracted major attention as their well-defined structure can help establish structure-function relationships. Indeed, structural variations of the molecular complex introduced, for instance, through synthetic modification of the ligands can allow fine-tuning of the complex reactivity, as well as understanding of the key steric and electronic effects on operating mechanism, product selectivity, and catalytic efficiency.[8,11–28] Up to date, very few studies have characterized the effects of ligand substituents on the performances of a given class of molecular CO_2 reduction catalysts, based on a significant set of representatives.[18–20,25–30] Product selectivity in CO_2 reduction is one of the most important issues to be addressed.[31–36] While in general molecular catalysis is limited to 2-electron reduction leading to formic acid and/or carbon monoxide, a major competing reaction is the reduction of protons into dihydrogen.[10,37] Optimization of the catalytic systems thus requires a better understanding of the factors which would limit the hydrogen evolution reaction. Knowledge on how it can be controlled is essential for the design and development of more efficient and selective CO_2 reduction catalysts.

Recently we have addressed this specific issue in the case of Co-terpyridine complexes, which catalyze the electroreduction of CO_2 into CO, while simultaneously performing a significant proton reduction into hydrogen.[18] The work demonstrated how simple variations in substituents on the terpyridine (terpy) ligand can have major effects on the CO/H_2 product ratio.[18] Specifically, using 5 differently substituted terpy ligands, we showed that electronic tuning of the ligand sphere had greater effect on proton reduction rates relative to CO_2 reduction rates. As a consequence, electron-withdrawing groups disfavored H^+ reduction, thus led to an increased selectivity for CO_2 reduction. These findings validated the concept of "turning off" proton reduction, in order to gain increased selectivity for CO_2-derived products. However, Co-terpy systems suffered from low efficiency (low Faradic yields) and significant instability and could not be studied further.

While the great majority of molecular CO_2 reduction catalysts convert CO_2 into CO, only very few have been reported as catalysts for the reduction of CO_2 to formic acid.[37,38] Well-known examples are Ru-polypyridyl, $Mn(bpy)(CO)_3$ and Rh(bpy=2,2′-bipyridine)(Cp^*=pentamethylcyclopentadienyl) complexes, followed recently by Co(diphosphine)(Cp) complexes[30] and Fe-carbonyl clusters.[32–35] These systems most often give a mixture of HCOOH and H_2, but the control of their selectivity has not been addressed in details.

In this context, the $[Rh(bpy)(Cp^*)X]^+$ catalyst is of particular interest for several reasons. It has been studied extensively for the reduction of a wide range of substrates (protons, ketones, NAD^+ and flavins) either by a hydride donor (such as formate) or *via* electrochemical or photochemical reduction in the presence of protons.[39,40] Initially, Kölle and Grätzel have shown that this rhodium-based system could catalyze photochemical hydrogen generation by using weakly reducing electrons of a TiO_2 colloid.[41] Subsequently, Deronzier et al.[42–44] and Gray et al.[45–47] have used $[Rh(bpy)(Cp^*)X]^+$-derived catalysts both in homogeneous solution or immobilized on electrode to study the electrochemical proton reduction to hydrogen. On the other hand, electrocatalytic CO_2 reduction by this catalyst was investigated for the first time by Deronzier and co-workers in 1997, reporting the formation of a mixture of formate and hydrogen.[48] Then, the system was left aside for almost 20

years until we used it for the first time as a catalyst for CO_2 photochemical reduction, in the presence of a photosensitizer and a sacrificial electron donor, also observing formate as the only carbon-containing product together with H_2.[48] With TONs above 100, this stable system compares well with Ru- and Mn-based photosystems.[38] It thus offers an interesting opportunity to carry out a structure-selectivity study aiming at understanding how to tune the HCOOH : H_2 ratio by varying the electronic nature of substituents on the bpy ligand. In this work, a series of [Rh(R-bpy)(Cp*)Cl]Cl organometallic complexes (R = OCH_3, CH_3, H, $COOC_2H_5$, CF_3, NH_2 and COOH) have thus been synthesized, characterized by cyclic voltammetry in order to probe the electronic properties of the bpy substituents, and compared in terms of the obtained HCOOH : H_2 ratio using photochemical conditions.

Another reason for studying this class of complexes is the existence of two potential active intermediates which have been studied, however only during proton electroreduction to H_2.[40,47,51] It was established that the metal center acts as the primary site of proton capture generating a metal hydride, but subsequently the latter tautomerizes by proton transfer to the Cp* ligand, giving rise to the thermodynamically more favorable (Cp*H)Rh(bpy) form.[40,47,51] The resulting species bearing the uncommon [η^4-Cp*H] ligand was isolated and structurally characterized by X-ray diffraction and ^{1}H NMR spectroscopy.[47,40] In turn, these findings opened a new question regarding the way such a catalyst mediates hydride transfer to an electrophilic substrate: indirectly *via* a Rh–H intermediate or directly from the [Cp*H] moiety of the cyclopentadiene ligand. In the case of H_2 evolution or NAD^+ reduction, the suggested scenario includes an intramolecular hydride transfer to the Cp* ring, followed by binding of the substrate (H^+ or NAD^+) to the metal center.[40,47]

We here extend these studies to CO_2 reduction. Our work is the first theoretical assessment of the mechanistic pathways for CO_2 reduction catalyzed by this class of complexes. Combining photochemical CO_2 reduction catalytic assays using [Rh(R-bpy)(Cp*)Cl]Cl complexes to assess the effect of the R substituents on the HCOOH : H_2 ratio with density functional theory (DFT) computations, we establish a structure-function relationship which can be used to tune the selectivity of the CO_2 reduction. Our calculations identify the respective roles of the two hydride tautomers in CO_2 *vs.* proton reduction and provide an understanding on how the presence of electron-withdrawing or donating moieties on the bpy ligand can affect the operating mechanism and the product selectivity of the Rh(R-bpy)(Cp*) catalysts.

RESULTS AND DISCUSSION

Preparation and characterization of Rh complexes. Eight [Rh(R-bpy)(Cp*)Cl]Cl complexes, R being a substituent group in the 4,4′ positions of bipyridine (H, CH_3, OCH_3, NH_2, COOH, $COOC_2H_5$ and CF_3) or a 5,5′-COOH group, were prepared according to previously reported methods.[41] Structures of the catalysts investigated in this study are shown in Scheme 1. Bipyridine (complex **C1**) was functionalized with seven electron-donating (complexes **C2**–**C4**: CH_3, OCH_3 and NH_2, respectively) or electron-withdrawing (complex **C5:** COOH at *meta* positions, complexes **C6**–**C8**: COOH, $COOC_2H_5$, and CF_3 groups at *para* positions, respectively) substituents. After purification, they were characterized by elemental analysis and NMR spectroscopy (see Experimental methods).

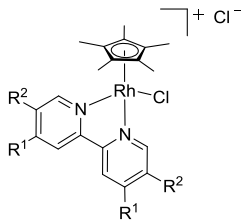

C1: R^1 = H R^2 = H
C2: R^1 = CH_3 R^2 = H
C3: R^1 = OCH_3 R^2 = H
C4: R^1 = NH_2 R^2 = H
C5: R^1 = H R^2 = COOH
C6: R^1 = COOH R^2 = H
C7: R^1 = $COOC_2H_5$ R^2 = H
C8: R^1 = CF_3 R^2 = H

Scheme 1. Structure of [Rh(R-bpy)(Cp*)Cl]Cl complexes.

Cyclic Voltammetry in Ar. First, the complexes were studied *via* cyclic voltammetry (CV) under Ar to assess the effect of the electronic nature of the bpy substituents. Figure 1 summarizes the CVs of all **C1**–**C8** complexes, with the potentials reported *vs.* $Fc^{+/0}$ (ferrocene was added as an internal standard to the solution after each measurement). The potential values for all complexes are given in Figure S1. As previously reported,[33,46–48] **C1** displays a single 2-electron reduction wave centered at –1.18 V *vs.* $Fc^{+/0}$, with a peak-to-peak separation (ΔE_p) of 120 mV, indicating electrochemical quasi-reversibility. This wave has already been assigned,[48] and here confirmed by DFT orbital analysis to correspond to a metal-based reduction of Rh(III) to Rh(I), accompanied by the loss of the labile chloride ligand. Complexes **C2** and **C3** also display such a single virtually reversible 2-electron reduction feature assigned to Rh(III)/Rh(I) but, owing to the electron-enriched bpy ligands, it occurs at slightly more cathodic potentials of –1.22 and –1.28 V, respectively. Additionally, the charge in these systems results in a smaller ΔE_p value of 80 and 70 mV, respectively. The CV of the most electron-donating complex **C4** that has NH_2 substituents on the bpy ligands is characterized by two separate one-electron reduction features centered at –1.23 and –1.53 V, with ΔE_p values of 240 and 60 mV, respectively, indicating that only the Rh(II)/Rh(I) couple is reversible.

The CV profiles of the electron-withdrawing complexes **C5**–**C8** are substantially different from the parent complex (**C1**) or the electron-donating **C2**–**C4**, notably with a significant or complete loss of reversibility. In the case of **C5**, the COOH substituents are at *meta* position and have thus more substantial impact on the electronic properties of bpy ligand compared to **C6** with –COOH groups at *para* position. The CV of **C5** is more complex, showing two reduction features with cathodic potentials at $E_{pc}' = -1.11$ V and $E_{pc}'' = -1.74$ V *vs.* $Fc^{+/0}$. The 130 mV anodic shift of the first reduction potential with respect to the unsubstituted complex **C1** reflects the strong electron-withdrawing nature of the *meta* COOH group. The second reduction wave is strongly cathodically shifted, which might be due to the involvement of the Cl ligand in the coordination sphere.

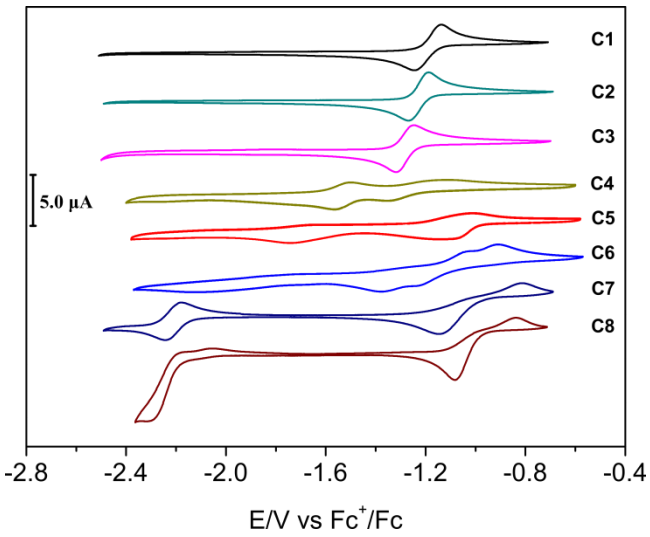

Figure 1. Cyclic voltammetry of **C1**–**C8** complexes in acetonitrile with 0.1 M $TBAPF_6$ as an electrolyte under Ar and a scan rate of 100 mV s^{-1}.

In complex **C6**, the two consecutive one-electron metal-based reduction waves are electrochemically irreversible, with E_{pc} = –1.23 and –1.36 V *vs.* $Fc^{+/0}$. The CV of complex **C7** is characterized by one irreversible reduction at E_{pc} = –1.14 V *vs.* $Fc^{+/0}$, while in the anodic scan, the product is reoxidized at E_{pa} = –0.82 V. A third one-electron reversible reduction event is observed at $E_{1/2}$ = –2.23 V and is associated with the reduction of the bpy-$COOC_2H_5$ ligand. Very similar electrochemical features are seen for complex **C8**, for which the more electron-withdrawing $–CF_3$ substituent groups on the bpy shift the irreversible reduction more anodically to E_{pc} = –1.08 V *vs.* $Fc^{+/0}$, while the reoxidation occurs at E_{pa} = –0.84 V. However, in contrast to **C7**, the third reduction of this complex results in an irreversible wave at E_{pc} = –2.28 V. The general trend evident from Figure 1 is that increasing the electron-withdrawing character of the functional group on the bpy ligand in the [Rh(R-bpy)Cp*] complex, increases the irreversibility of the Rh(III)/Rh(I) reduction. A possible reason could be the strong stabilization of the Rh(I) complex, resulting from the enhanced delocalization of electron density, which makes in turn more difficult to oxidize it to the Rh(III) form. Similar electrochemical behavior for complexes with *para* substituted –tBu and $–CF_3$ on the bpy ligand in $[Rh(bpy)Cp^*Br]^+$ system was reported recently by Blakemore et. al. in their studies on the role of the ligand substituents on the proton reduction activity.[52]

The potential of the first cathodic peak was used as a measure of the electronic properties of the substituted bpy ligands. Figure 2 shows that under Ar it spans over a 270 mV range and correlates almost linearly (R^2 = 0.95) with the values of the Hammett sigma parameter,[55] in the following order: NH_2 > OCH_3 > CH_3 > H > *m*-COOH > $COOC_2H_5$ > CF_3. The *para* substituted COOH complex (**C6**) falls off the line (blue square in Figure 2), as its reduction is more difficult than that of the corresponding ester (**C7**), despite the same Hammett constant values. This is possibly due to surface adsorption of **C6** on the glassy carbon electrode as shown from a rinse test (Figure S2). Similar findings for linear relationship between the first reduction potential and the Hammett parameter were reported for Ru-bis-diimine complexes by Connick and co-workers[56] as well as for a series of *fac*-Re(4,4′-R-bpy)$(CO)_3X$ catalysts by Kubiak and co-workers.[27] One should note that the range of accessible potentials in this work (over 270 mV) is much lower than that obtained with Co-bisterpyridyl complexes (over 1V),[57] reflecting the weaker sensitivity of the $[Rh(R\text{-}bpy)(Cp^*)]^+$ systems to the electronic effects introduced *via* electron-withdrawing or donating functional groups on the bpy ligand.

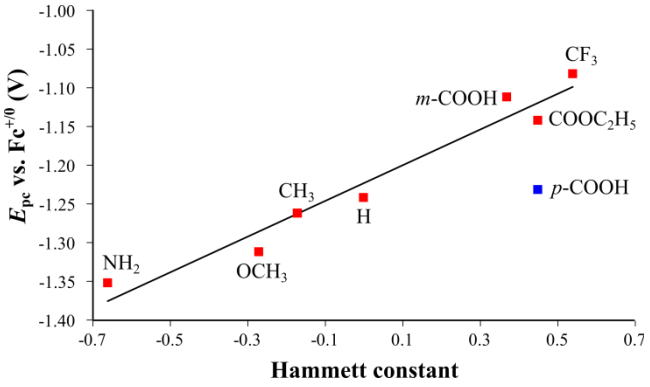

Figure 2. Trend between the electron-donating character of the bpy substituent and the first cathodic peak potential (E_{pc}) of complexes **C1**–**C8**. Blue square corresponds to **C6**.

Photoreduction of Carbon dioxide. The catalytic performance of the **C1**–**C8** complexes was studied towards photochemical CO_2 reduction under conditions described in the experimental section. As the complexes are not photocatalysts they need to be sensitized. The $[Ru(bpy)_3]^{2+}$ complex was used as a photosensitizer. Because of the larger extinction coefficient in the visible light region and larger concentration of the Ru complex with respect to the Rh-based catalysts, inefficient light absorption by the photosensitizer was excluded.[58] Furthermore, triethanolamine (TEOA) was used the electron donor and the proton source, as generally done in photochemical CO_2 reduction of molecular systems.[59] H_2 and HCOOH were detected as reduction products. Control experiments did not show any significant activity when the reaction was carried out in the dark as well as in the absence of $[Rh(R\text{-}bpy)(Cp^*)Cl]^+$ catalysts or $[Ru(bpy)_3]Cl_2$ photosensitizer, thus confirming that the Rh complexes are not photocatalysts (Figure S3).

The performance of **C1**–**C8** complexes was compared in terms of initial turnover frequency (TOF) obtained within 1 h of reaction and turnover numbers (TON) after 16 hours (Table 1). Figure 3 depicts the representative complexes **C3** (a) and **C8** (b) in terms of TON for each product as a function of time. The curves obtained for the other six complexes are summarized in the SI section (Figures S4-S9). The initial linear part of the curve was used to calculate a TOF value for each product. Both products (HCOOH and H_2) form immediately upon illumination, with a reaction rate that does not vary significantly during the first two hours. After 2h, the rate slowly decays with time as a consequence of photosensitizer bleaching. This is supported by the observed recovery of catalytic activity upon addition of fresh sample of $[Ru(bpy)_3]Cl_2$ during irradiation.[49]

Complexes **C1**–**C3** that have electron-enriched bpy ligands show similar properties: (i) they produce formic acid

with the highest TON values (above 100) in the order **C3** > **C1** > **C2**, and have the highest initial TOF values (about 30 h^{-1}) and (ii) they are the most selective catalysts for CO_2 reduction among the set of catalysts under study here (highest value of TOF(HCOOH) : TOF(H_2) of 1.36).

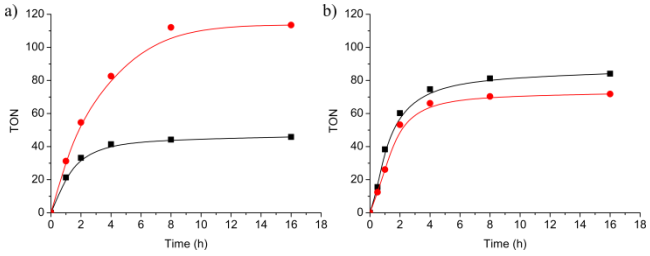

Figure 3. Formate (red) and H_2 (black) evolution catalyzed by a 0.1 mM solution of **C3** (a) and **C8** (b) in the presence of 1 mM of $[Ru(bpy)_3]Cl_2$ in CO_2-saturated CH_3CN/TEOA (5:1, v/v) mixture upon irradiation with a 300 W Xe arc lamp equipped with a 415 nm filter.

In sharp contrast, complexes **C4**–**C8** show much weaker catalytic activity for CO_2 reduction. Among them, a sub-class of **C4**–**C6** emerges as systems with special catalytic properties, which do not follow the general trend (*vide infra*), due to the presence of protic substituents (–COOH and $–NH_2$). They are characterized by (i) very low catalytic activity for CO_2 reduction, as illustrated by the very low TON and TOF values (Table 1) and (ii) production of H_2 as a major product. On the other hand, complexes **C7** and **C8** that have the most electron-deficient ligands and no protic groups on the bpy ligand produce similar amount of products, with a HCOOH : H_2 ratio of about 1 : 1. Interestingly, substitution of the –COOH group (**C6**) by $–COOC_2H_5$ (**C7**) leads to a two-fold increase of the formate production rate, while the H_2 evolution rate is only marginally enhanced, resulting in two-fold increase of the HCOOH : H_2 ratio.

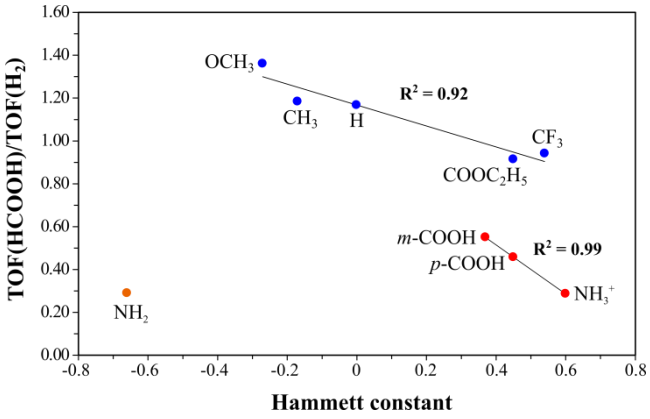

Figure 4. TOF(HCOOH)/TOF(H_2) ratio as a function of the Hammett constant (σ) of the functional groups on the bpy ligand for [Rh(R-bpy)(Cp*)Cl]Cl complexes **C1**–**C8**.

Our photochemical results demonstrate that electronic modifications on the bpy ligand of [Rh(R-bpy)(Cp*)Cl]Cl catalysts have a significant effect on product selectivity, measured in terms of TOF(formate)/TOF(H_2), and ranging from 1.36 to 0.29. Moreover, selectivity correlates almost linearly (R^2 = 0.92) with the Hammett constant (σ), hence with the cathodic potential for the Rh(III)/Rh(I) couple (Figure 2), used as a descriptor of the electronic effect of the substituents (Figure 4), with the exception of complexes **C4**–**C6**. **C4**, with the most electron-donating bpy ligand (σ = –0.66) was expected to show the highest selectivity for formic acid. Instead, the lowest selectivity that it shows likely reflects the fact that the $–NH_2$ substituents are protonated by the large excess of TEOA. Thus in Figure 4 we also plotted **C4** in the NH_3^+ state (σ = +0.60), which greatly improves the correlation (R^2 = 0.99) among the **C4**–**C6** systems. Figure 4 also suggests that there are two classes of catalysts, displaying two different linear trends. Within each class, increasing the electron-donating nature of the bpy ligand increases the selectivity of the catalyst for formic acid production. It should be noted that **C4**–**C6** complexes differ from the others by the presence of proton-exchange groups. Whether this explains their greater propensity to reduce protons has to be considered even though intramolecular processes seem unlikely due to the large distance between these substituents and the metal center.

Table 1. Results of photolytic CO_2 reduction catalyzed by [Rh(R-bpy)(Cp*)Cl]Cl complexes and the $[Ru(bpy)_3]Cl_2$ photosensitizer, given in terms of initial TOF and TON after 16 hours reaction.

Catalyst	TON_{16h}		$TOF\ (h^{-1})$		Selectivity
	formate	H_2	formate	H_2	
C1 (R = H)	105.2	63.3	31.4	26.9	1.17
C2 (R = CH_3)	99.5	51.8	26.4	22.3	1.18
C3 (R = OCH_3)	113.5	45.8	32.1	23.6	1.36
C4 (R = NH_2)	21.5	68.3	7.7	26.9	0.29
C5 (R = *m*-COOH)	38.3	49.2	11.1	20.2	0.55
C6 (R = *p*-COOH)	31.2	64.6	11.7	25.6	0.46
C7 (R = $CO_2C_2H_5$)	69.8	77.9	25.5	27.9	0.91
C8 (R = CF_3)	71.8	84.1	28.7	30.5	0.94

We found that **C4**–**C6** catalysts show very low CO_2 reduction ability and strong tendency to favor H_2 formation. Recently, Monte Carlo simulating annealing coupled with DFT calculations revealed that upon immobilization of complexes **C4** or **C5** into the porous metal-organic framework MIL-101-NH_2(Al), the –COOH groups of the Rh system can establish hydrogen bonding interactions with the MOF host (with an $–NH_2$ group of the neighboring linker and/or H_2O molecule of an inorganic sub-unit).[50] Since the immobilized Rh-Ru@MIL-101-NH_2(Al) composite performed photochemical CO_2 reduction to produce exclusively formate, the MOF host was recognized as a key component in altering the selectivity of the catalyst achieved by inhibiting the competing proton reduction.[50] In contrast, the photochemical reduction of the homogeneous complexes **C4**–**C6** in this work showed the formation of hydrogen as a main product, with little amount of formic acid (Table 1), which could indicate the involvement of the carboxylic groups (as well as $–NH_3^+$ groups) in H_2 formation

via a reaction path that is suppressed when immobilized in the MOF host. Further studies are required to better understand this behavior.

Finally, the relationship depicted in Figure 4 reveals a direct molecular-level influence of the functional group on the initial reaction rate for CO_2 *vs.* proton reduction reactions. It can be used to predict the product selectivity of other [Rh(R-bpy)(Cp*)] complexes based on the corresponding Hammett constant value of the R group.

Density functional theory calculations. DFT calculations were performed in order to investigate the mechanistic pathways for CO_2 reduction to HCOOH and proton reduction to H_2 by this class of catalysts, as well as to assess the role of substituents on the bipyridine ligand on the product selectivity. To the best of our knowledge, there have been no DFT studies on the CO_2 reduction to formate by $[Rh(R\text{-}bpy)(Cp^*)]^+$ systems reported in the literature. In terms of proton reduction to hydrogen, the only computational work addresses the unsubstituted [Rh(bpy)(Cp*)Cl]Cl complex.[51] Here, we go a step further to investigate the effect of the substituent on the bpy ligand on the H_2 evolution mechanism and on the catalyst selectivity.

As revealed by the CV data and in agreement with previous electrochemical experiments on the unsubstituted $[Rh(bpy)(Cp^*)X]^+$ catalyst (**C1**)[43,44,53] and very recently on $[Rh(R\text{-}bpy)(Cp^*)X]^+$ with R = –tBu and $–CF_3$,[52] initially, a two-electron metal-centered reduction of Rh^{III} to Rh^{I} takes place (see Figures S18-S19), accompanied by a release of the halogen ligand. The computations were performed on complexes **C3** and **C8**, chosen as representatives of the [Rh(R-bpy)(Cp*)Cl]Cl catalysts functionalized with electron-donating and withdrawing groups, respectively.

First proton-transfer step. We started by computing the possible reaction pathways for the protonation of the initial two-electron reduced complex **1** (Figure 5). Et_3NH^+ was used in the calculations as a model of triethanolammonium ion derived from TEOA.[59,60] Complex **1** is a Rh(I) complex, most favorably protonated at the metal site to form a Rh(III)-H hydride species, complex **2**, with a transition state barrier ($TS_{1\text{-}2}$) of only 3.6 kcal mol^{-1} for **C3** and 10.3 kcal mol^{-1} for **C8**. Direct protonation at the Cp* ring forming an η^4-pentamethylcyclopentadiene ligand with the new C–H bond *endo* with respect to the metal center, requires much higher transition state barriers $TS_{1\text{-}3}$ of 21.6 and 27.4 kcal mol^{-1} for **C3** and **C8**, respectively. Hence, direct protonation of the Cp* ring is unlikely to occur. Formation of complex **2** is exergonic by 7 kcal mol^{-1} for the electron-donating complex **C3**, and endergonic by 6.9 kcal mol^{-1} for the electron-withdrawing **C8**. Next, the Rh(III)-hydride **2** has to undergo an intramolecular proton transfer to the Cp* ring, in order to form the thermodynamically stable species **3**. The $TS_{2\text{-}3}$ barrier is computed to be 17.2 and 12.8 kcal mol^{-1} for **C3** and **C8**, respectively, which indicates that the proton transfer from the Rh site to the Cp* ring is significantly easier in the presence of electron-withdrawing substituents. It should be noted that for all **C1**–**C8** systems the [RhH] form is always less stable than the [Cp*H] tautomer by about 2-3 kcal mol^{-1}, which is in agreement with the experimental isolation of (Cp*H)Rh(bpy) complex and subsequent characterization by X-ray crystallography and NMR spectroscopy.[40,47]

Reaction pathway for CO_2 reduction to formate. Then, we investigated the mechanistic pathways for the reduction of CO_2 to formate *via* the two key intermediates, i.e., complexes **2** and **3**, and established the role of the [RhH] *vs.* [Cp*H] moieties. Figure 6 shows that formate production occurs only from the Rh(III)-hydride species *via* a direct CO_2 attack to form a transition state $TS_{2\text{-}4}$ with a free energy of activation of 17.2 and 19.5 kcal mol^{-1} for **C3** and **C8**, respectively. The direct hydride transfer to form the $[Rh\cdots HCO_2^-]$ complex **4** is followed by further protonation and a release of HCOOH and the $[Rh^{III}(R\text{-}bpy)(Cp^*)]^{2+}$ complex **5** (ΔG = 4.4 and 23.1 kcal mol^{-1} for **C3** and **C8**, respectively). Complex **5** most likely binds a CH_3CN solvent molecule (the Gibbs free energies for this reaction are +2.6 (**C3**) and -0.9 (**C8**) kcal mol^{-1}). Further two-electron reduction recovers the catalytic active Rh^I species **1**. In contrast, CO_2 attack at the η^4-Cp*H complex **3** goes through much higher transition state barriers of 43 (**C3**) and 42 (**C8**) kcal mol^{-1} (see Figure 6). This clearly indicates the key role of the Rh(III)-hydride intermediate and excludes the [Cp*H] tautomer for the reduction of CO_2 to formate by the $[Rh^I(R\text{-}bpy)(Cp^*)]$ class of catalysts.

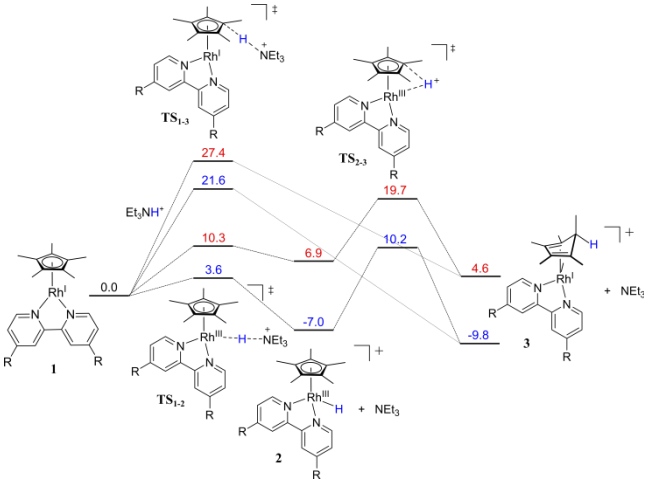

Figure 5. Reaction profile for the protonation of $[Rh^I(R\text{-}bpy)(Cp^*)]$, with R = $–OCH_3$ in blue and R = $–CF_3$ in red. Energies (in kcal mol^{-1}) are given with respect to complex **1**.

The lower TS barrier for the rate-limiting step of direct hydride transfer to CO_2 corroborates the experimental findings that $[Rh^I(R\text{-}bpy)(Cp^*)]$ complexes containing electron-donating groups at the bpy ligand are better CO_2 reduction catalysts than those with electron-withdrawing substituents in terms of producing more formate.

Reaction pathway towards hydrogen formation. The second main product observed in our photochemical reduction experiments on $[Rh(R\text{-}bpy)(Cp^*)Cl]^+$ catalysts is resulting from the competitive proton reduction reaction leading to the formation of hydrogen. Up to date, most of the research efforts have focused on the hydrogen production by the unsubstituted complex **C1**[41,47,51,54] and, only very recently, Blakemore et. al. have reported electrochemical H_2 formation by complexes with *para* substituted –tBu and $–CF_3$ on the bpy ligand in $[Rh(bpy)Cp^*Br]^+$ system.[52] Electrochemical proton reduction studies revealed that 1 equiv. of acid results in transfer of proton to the Cp* ring, creating the [Cp*H] intermediate **3**, which is suggested to play a key role for hydrogen evolution

upon addition of more acid.[47,52,54] Furthermore, DFT computations by S.I. Johnson et al. demonstrated the role of the acid strength in assessing different reaction mechanisms, and that H_2 forms only upon direct attack of strong acid on the Rh(III)-H bond.[51] In this work, we computed the H_2 evolution reaction mechanism as a function of the substituent groups on the bpy ligand, in order to assess how their electronic nature affects the competition between HCOOH and H_2.

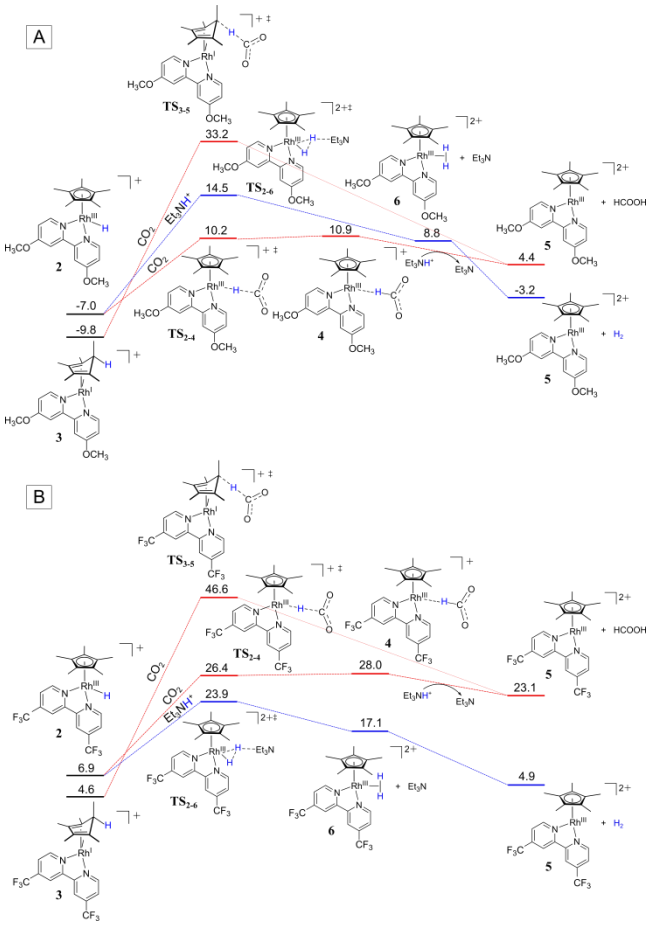

Figure 6. Reaction profile for CO_2 reduction to formate (pathway in red) and H_2 formation (in blue), for complex **C3** (top panel A) and **C8** (bottom panel B). Energies (in kcal mol^{-1}) are given with respect to complex **1**.

As shown in Figure 6, both complexes **C3** and **C8** form hydrogen from a direct attack of the acid on the Rh–H bond, leading to an H–H bond in a RhH_2 adduct **6**, followed by a release of H_2 and the $[Rh^{III}(R\text{-bpy})(Cp^*)]^{2+}$ complex **5** (ΔG = –3.2 and 4.9 kcal mol^{-1} for **C3** and **C8**, respectively). The transition state barriers $TS_{2\text{-}6}$ amount to 21.5 (**C3**) and 17 (**C8**) kcal mol^{-1}. Hydrogen evolution pathway *via* the [Cp*H] tautomer involving an acid attack at the Rh(I) center that generates the Rh(III)H(Cp*H) species proceeds through an intramolecular H–H interaction (Figures S20 and S21). While this step has virtually the same TS barrier (21.3 kcal mol^{-1}) as that originating from the direct attack on the Rh–H bond for **C3**, it amounts to 24.8 kcal mol^{-1} for **C8**. As such, our calculations suggest that this reaction pathway might be operational for complexes with electron-donating substituents, but highly unlikely for the electron-withdrawing ones.

Interestingly, we observe an inversion in the transition state energies: in the case of **C3** the lowest barrier is computed for the hydride transfer to CO_2 ($TS_{2\text{-}4}$ of 17.2 *vs* 19.5 kcal mol^{-1}), while for **C8** it is for the hydride transfer to protons ($TS_{2\text{-}6}$ of 17 *vs* 21.5 kcal mol^{-1}). Thus decreasing the electron density on bipyridine (here from **C3** to **C8**) results in opposite effects on the computed energies of the transition states of the rate-determining step of the reduction reactions, i.e., TS barrier for proton reduction decreases, while the barrier for the CO_2 reduction increases. This trend is in excellent agreement with the experimental observation that during the photochemical CO_2 reduction, the HCOOH : H_2 ratio decreases from **C3** to **C8**, thus recognizing the complexes with electron-donating functionalized ligands as more selective catalysts for formate production.

Several studies have recognized the importance of hydricity of the intermediate hydride species as a descriptor of the CO_2 *vs* H^+ selectivity.[33–36,61–65] Here, the computed hydricity values for **C3** and **C8** are 70.8 and 74.8 kcal mol^{-1}, respectively (see the Supporting Information for the employed protocol). These values are significantly higher than the hydricity of $HCOO^-$ (45.1 kcal mol^{-1} computed in this work, 43 kcal mol^{-1} reported experimentally[66]). However, if the Rh complex is further reduced by one electron, the corresponding hydricities become 43.1 (**C3**) and 51 (**C8**) kcal mol^{-1}. Interestingly, the transition state barriers for the hydride transfer from the $[Rh^{III}H(R\text{-bpy}^{\cdot-})(Cp^*)]^0$ complex upon CO_2 attack are lowered by only ~2 kcal mol^{-1} to 15.4 and 17.4 kcal mol^{-1} for **C3** and **C8**, respectively. As such, these hydricity values are consistent with **C3** being a better CO_2 reduction catalyst.

CONCLUSIONS

In this work, we studied the photochemical CO_2 reduction to formic acid catalysed by a series of $[Rh(R\text{-bpy})(Cp^*)Cl]^+$ complexes, with R being a substituent group in the 4,4′ positions of bipyridine (H, CH_3, OCH_3, NH_2, COOH, $COOC_2H_5$ and CF_3) or a 5,5′-COOH group. This study aimed at using variously substituted ligands in order to fine-tune the selectivity of the catalyst, defined as the HCOOH : H_2 product ratio. The first cathodic peak potential of the complexes was found to correlate linearly with the values of the Hammett parameter of the substituents, in the following order NH_2 > OCH_3 > CH_3 > H > *m*-COOH > $COOC_2H_5$ > CF_3, spanning 270 mV range from NH_2 to CF_3. While this range is small, the $[Rh(R\text{-bpy})(Cp^*)]^+$ series of complexes was appropriate for correlating the catalytic activity with the electronic properties of the coordination sphere.

We experimentally demonstrated the general trend that electronic modifications at the bpy ligand have a significant effect on product selectivity and that two classes of catalysts can be identified, which display two different linear trends. More specifically, we showed that increasing the electron-donating nature of the bpy ligand increases the HCOOH : H_2 product ratio. Among the systems investigated in this work, $[Rh(OCH_3\text{-bpy})(Cp^*)Cl]^+$ was found to be the most selective catalyst for formic acid production. Our DFT calculations rationalized the observed tendency of electron-donating substituents to favor CO_2 reduction by means of lowering the hydride transfer barrier towards formate production as compared to electron-withdrawing substituents that favor more strongly the proton reduction to hydrogen. Similar strategies have been proposed in order to alter the electronics of Mn and Fe catalysts for CO_2 hydrogenation.[67,68] In addition, we have clarified for the first time the respective role of the [RhH] *vs.*

[Cp*H] tautomers in CO_2 *vs*. proton reduction, recognizing the Rh(III)-hydride as the key player in both reactions.

EXPERIMENTAL METHODS

All starting materials and solvents were commercially available and were used without further purification. ^{1}H NMR spectra were recorded on a Bruker Avance III 300 NMR spectrometer at room temperature. FT-IR spectra were recorded on a IR Prestige-21 spectrometer (Shimadzu, Kyoto, Japan); the spectra are given in Figures S10-S17 in the Supporting Information.

Synthesis of Cp*Rh(bpy)Cl$_2$·H$_2$O (C1). A 50 mL reaction flask was charged with 0.506 g (0.820 mmol, 1 equiv) of $[Cp^*RhCl_2]_2$, 0.256 g (1.64 mmol, 2 equiv) of 2,2′-bipyridine, and 25 mL of MeOH. The mixture was allowed to stir at room temperature for 1 hour. The reaction mixture became fully homogeneous over an hour of the experiment and the solution obtained an orange color. The reaction mixture was concentrated *in vacuo*. Excess diethyl ether was added to the reaction flask to yield an orange precipitate complex **C1**, which was further collected on a Buchner funnel and dried under vacuum (92%). ^{1}H NMR (300 MHz, CD_3CN): δ(ppm) 8.89 (d, J = 5.4 Hz, 2H), 8.44 (d, J = 8.0 Hz, 2H), 8.29-8.18 (m, 2H), 7.81 (t, J = 6.6 Hz, 2H), 1.66 (s, 15H). ^{13}C NMR (75 MHz, CD_3CN): δ(ppm) 154.37, 15.00, 140.31, 128.36, 123.92, 97.29 (d, $^1J_{C,Rh}$ = 8.25 Hz, Cp*), 8.18 (CH_3(Cp*)). ESI-MS(+) (CH_3CN): *m*/*Z* calcd for $C_{20}H_{23}ClN_2Rh$ 429.06, found 429.2 (M^+). FT-IR (CD_3CN): ν_{max} (cm^{-1}) 3634, 3542, 2106, 1632, 1606, 1493, 1473, 1448, 1386, 1381, 1311, 1248. *Anal.* Calcd. for $C_{20}H_{25}N_2Cl_2ORh$ (483.24): C 49.71, H 5.21, N 5.80; Found: C 49.51, H 4.94, N 5.69.

Synthesis of Cp*Rh(4,4′-CH$_3$-bpy)Cl$_2$·H$_2$O (C2). A 50 mL reaction flask was charged with 0.506 g (0.820 mmol, 1 equiv) of $[Cp^*RhCl_2]_2$, 0.302 g (1.64 mmol, 2 equiv) of 4,4′-methyl-2,2′-bipyridine, and 25 mL of MeOH. The mixture was allowed to stir at room temperature for 1 hour. The reaction mixture became fully homogeneous over an hour of the experiment and the solution obtained an orange color. The reaction mixture was concentrated *in vacuo*. Excess diethyl ether was added to the reaction flask to yield an orange precipitate complex **C2**, which was further collected on a Buchner funnel and dried under vacuum (89%). ^{1}H NMR (300 MHz, CD_3CN): δ(ppm) 8.70 (d, J = 5.7 Hz, 2H), 8.28 (s, 2H), 7.61 (d, J = 4.8 Hz, 2H), 2.58 (s, 6H),1.65 (s, 15H). ^{13}C NMR (75 MHz, CD_3CN): δ(ppm) 154.06, 152.99, 151.11, 128.95, 124.41, 96.94 (d, $^1J_{C,Rh}$ = 8.25 Hz, Cp*), 20.41 (CH_3(4,4′-CH_3-bpy)), 8.16 (CH_3(Cp*)). ESI-MS(+) (CH_3CN): *m*/*Z* calcd for $C_{22}H_{27}ClN_2Rh$ 457.09, found 457.2 (M^+). FT-IR (CD_3CN): ν_{max} (cm^{-1}) 3631, 3544, 1622, 1558, 1486, 1455, 1420, 1381, 1321, 1302, 1282, 1244, 1223. *Anal.* Calcd. for $C_{22}H_{29}N_2Cl_2ORh$ (511.29): C 51.68, H 5.72, N 5.48; Found: C 51.69, H 5.48, N 5.38.

Synthesis of Cp*Rh(4,4′-OCH$_3$-bpy)Cl$_2$·2H$_2$O (C3). A 50 mL reaction flask was charged with 0.506 g (0.820 mmol, 1 equiv) of $[Cp^*RhCl_2]_2$, 0.355 g (1.64 mmol, 2 equiv) of 4,4′-methoxyl-2,2′-bipyridine, and 25 mL of MeOH. The mixture was allowed to stir at room temperature for 1 hour. The reaction mixture became fully homogeneous over an hour of the experiment and the solution obtained an orange color. The reaction mixture was concentrated *in vacuo*. Excess diethyl ether was added to the reaction flask to yield an orange precipitate complex **C3**, which was further collected on a Buchner funnel and dried under vacuum (91%). ^{1}H NMR (300 MHz, CD_3CN): δ(ppm) 8.63 (d, J = 6.5 Hz, 2H), 7.96 (d, J = 2.7 Hz, 2H), 7.30 (dd, J = 6.5, 2.7 Hz, 2H), 4.07 (s, 6H),1.64 (s, 15H). ^{13}C NMR (75 MHz, CD_3CN): δ(ppm) 168.63, 155.86, 152.55, 114.47, 110.33, 96.55 (d, $^1J_{C,Rh}$ = 8.25 Hz, Cp*), 57.09 (CH_3(4,4′-OCH_3-bpy)), 8.16 (CH_3(Cp*)). ESI-MS(+) (CH_3CN): *m*/*Z* calcd for $C_{22}H_{27}ClN_2O_2Rh$ 489.08, found 489.2 (M^+). FT-IR (CD_3CN): ν_{max} (cm^{-1}) 3629, 3542, 2108, 1617, 1563, 1498, 1473, 1441, 1422, 1339, 1313, 1282, 1270, 1257, 1230. *Anal.* Calcd. for $C_{22}H_{31}N_2Cl_2O_4Rh$ (561.31): C 47.08, H 5.57, N 4.99; Found: C 47.33, H 5.16, N 5.08.

Synthesis of Cp*Rh(4,4′-NH$_2$-bpy)Cl$_2$·2H$_2$O (C4). A 50 mL reaction flask was charged with 0.506 g (0.820 mmol, 1 equiv) of $[Cp^*RhCl_2]_2$, 0.305 g (1.64 mmol, 2 equiv) of 4,4′-amino-2,2′-bipyridine, and 25 mL of MeOH. The mixture was allowed to stir at room temperature for 1 hour. The reaction mixture became fully homogeneous over an hour of the experiment and the solution obtained an orange color. The reaction mixture was concentrated *in vacuo*. Excess diethyl ether was added to the reaction flask to yield an orange precipitate complex **C4**, which was further collected on a Buchner funnel and dried under vacuum (81%). ^{1}H NMR (300 MHz, DMSO-d_6): δ(ppm) 8.19 (d, J = 1.6 Hz, 2H), 7.20-7.04 (m, 6H), 6.81 (dd, J = 6.5, 2.4 Hz, 2H), 1.58 (s, 15H). ^{13}C NMR (75 MHz, DMSO-d_6): δ(ppm) 157.05, 154.76, 151.22, 112.26, 106.38, 95.56 (d, $^1J_{C,Rh}$ = 7.5 Hz, Cp*), 8.89 (CH_3(Cp*)). ESI-MS(+) (CH_3CN): *m*/*Z* calcd for $C_{20}H_{25}ClN_4Rh$ 459.08, found 459.1 (M^+). FT-IR (d_6-DMSO): ν_{max} (cm^{-1}) 3499, 3431, 3338, 3187, 1658, 1623, 1558, 1506, 1479, 1464, 1370, 1354, 1270. *Anal.* Calcd. for $C_{20}H_{29}N_4Cl_2O_2Rh$ (531.28): C 45.21, H 5.50, N 10.55; Found: C 45.54, H 5.09, N 10.81.

Synthesis of Cp*Rh(5,5′-COOH-bpy)Cl$_2$·H$_2$O (C5). A 50 mL reaction flask was charged with 0.506 g (0.820 mmol, 1 equiv) of $[Cp^*RhCl_2]_2$, 0.400 g (1.64 mmol, 2 equiv) of 5,5′-carboxylic acid-2,2′-bipyridine, and 25 mL of MeOH. The mixture was allowed to stir at room temperature for 1 hour. The reaction mixture became fully homogeneous over an hour of the experiment and the solution obtained an orange color. The reaction mixture was concentrated *in vacuo*. Excess diethyl ether was added to the reaction flask to yield an orange precipitate complex **C5**, which was further collected on a Buchner funnel and dried under vacuum (81%). ^{1}H NMR (300 MHz, DMSO-d_6): δ(ppm) 9.27 (d, J = 1.6 Hz, 2H), 8.93 (d, J = 8.4 Hz, 2H), 8.76 (dd, J = 8.3, 1.8 Hz, 2H), 1.69 (s, 15H).). ^{13}C NMR (75 MHz, DMSO-d_6): δ(ppm) 164.53, 156.05, 152.40, 141.21, 131.71, 125.40, 97.78 (d, $^1J_{C,Rh}$ = 8.25 Hz, Cp*), 8.92 (CH_3(Cp*)). ESI-MS(+) (CH_3OH): *m*/*Z* calcd for $C_{22}H_{23}ClN_2O_4Rh$ 517.04, found 517.1 (M^+), 581.4 ($[M]^+$ + 2CH_3OH). ESI-MS(−) (CH_3OH): *m*/*Z* calcd for $C_{22}H_{21}ClN_2O_4Rh$ 515.02, found 515.1 ($[M-2H^+]^-$). FT-IR (d_6-DMSO): ν_{max} (cm^{-1}) 3499, 3442, 2913, 2778, 2602, 2478, 1914, 1710, 1668, 1611, 1593, 1428, 1377, 1278. *Anal.* Calcd. for $C_{22}H_{25}N_2Cl_2O_5Rh$ (571.26): C 46.26, H 4.11, N 4.90; Found: C 46.16, H 4.22, N 4.88.

Synthesis of Cp*Rh(4,4′-COOH-bpy)Cl$_2$·2H$_2$O (C6). A 50 mL reaction flask was charged with 0.506 g (0.820 mmol, 1 equiv) of $[Cp^*RhCl_2]_2$, 0.400 g (1.64 mmol, 2 equiv) of 4,4′-carboxylic acid-2,2′-bipyridine, and 25 mL of MeOH. The mixture was allowed to stir at room temperature for 1 hour. The reaction mixture became fully homogeneous over an hour of the experiment and the solution obtained an orange color. The reaction mixture was concentrated *in vacuo*. Excess diethyl ether was added to the reaction flask to yield an orange

precipitate complex **C6**, which was further collected on a Buchner funnel and dried under vacuum (83%). ^{1}H NMR (300 MHz, DMSO-d_6): δ(ppm) 9.19-9.06 (m, 4H), 8.21 (dd, J = 5.7, 1.5 Hz, 2H), 1.68 (s, 15H). ^{13}C{^{1}H} NMR (75 MHz, DMSO-d_6): δ(ppm) 165.19, 154.79, 153.64, 143.30, 127.87, 123.80, 97.97 (d, $^1J_{C,Rh}$ = 7.5 Hz, Cp*), 8.92 (CH_3(Cp*)). ESI-MS(+) (CH_3OH): *m*/*Z* calcd for $C_{22}H_{23}ClN_2O_4Rh$ 517.04, found 517.1 (M^+), 581.3 ($[M]^+$ + 2CH_3OH). ESI-MS(−) (CH_3OH): *m*/*Z* calcd for $C_{22}H_{21}ClN_2O_4Rh$ 515.02, found 515.1 ($[M-2H^+]^-$). FT-IR (d_6-DMSO): ν_{max} (cm^{-1}) 3492, 3441, 2916, 2777, 2457, 1908, 1712, 1664, 1558, 1480, 1446, 1401, 1315, 1280, 1257, 1234. *Anal.* Calcd. for $C_{22}H_{27}N_2Cl_2O_6Rh$ (589.27): C 44.24, H 4.25, N 4.65; Found: C 44.84, H 4.62, N 4.75.

Synthesis of Cp*Rh(4,4′-COOC$_2$H$_5$-bpy)Cl$_2$·2H$_2$O (C7). A 50 mL reaction flask was charged with 0.506 g (0.820 mmol, 1 equiv) of $[Cp^*RhCl_2]_2$, 0.492 g (1.64 mmol, 2 equiv) of 4,4′-ethyl carboxylate-2,2′-bipyridine, and 25 mL of MeOH. The mixture was allowed to stir at room temperature for 1 hour. Over on hour the reaction mixture was fully homogeneous and the solution obtained an orange color. The reaction mixture was concentrated on *in vacuo*. Excess diethyl ether was added to the reaction flask to yield an orange precipitate complex **C7**, which was further collected on a Buchner funnel and dried under vacuum (72%). ^{1}H NMR (300 MHz, DMSO-d_6): δ(ppm) 9.19 (m, 4H), 8.25 (d, J = 9 Hz, 2H), 4.49 (q, J = 6 Hz, 4H), 1.68 (s, 15H), 1.41 (t, J = 6 Hz, 6H). ^{13}C{^{1}H} NMR (75 MHz, DMSO-d_6): δ(ppm) 163.68, 154.77, 153.90, 141.24, 127.69, 123.84, 99.26 (d, $^1J_{C,Rh}$ = 7.5 Hz, Cp*), 63.02, 14.51, 9.06 (CH_3(Cp*)). ESI-MS(+) (CH_3OH): *m*/*Z* calcd for $C_{26}H_{31}ClN_2O_4Rh$ 573.1, found 573.2 (M^+). FT-IR (d_6-DMSO): ν_{max} (cm^{-1}) 3490, 3451, 2981, 1729, 1655, 1558, 1475, 1458, 1402, 1370, 1319, 1288, 1258, 1233. *Anal.* Calcd. for $C_{26}H_{35}N_2Cl_2O_6Rh$ (645.38): C 48.39, H 5.47, N 4.34; Found: C 48.40, H 5.51, N 4.31.

Synthesis of [Cp*Rh^{III}(4,4′-CF$_3$-bpy)Cl]Cl (C8). A 50 mL reaction flask was charged with 0.506 g (0.820 mmol, 1 equiv) of $[Cp^*RhCl_2]_2$, 0.479 g (1.64 mmol, 2 equiv) of 4,4'-bis(trifluoromethyl)-2,2'-bipyridine, and 25 mL of MeOH. The mixture was allowed to stir at room temperature for 1 hour. The reaction mixture became fully homogeneous over an hour of the experiment and the solution obtained a yellowish-orange color. The reaction mixture was evaporated *in vacuo* to obtain an oily residue. This residue was dissolved in 2 mL CH_3CN, followed by addition of excess diethyl ether to it to yield a yellow precipitate complex **C8**, which was further collected on a Buchner funnel and dried under vacuum (80%). ^{1}H NMR (300 MHz, CD_3CN): δ(ppm) 9.15 (d, J = 5.4 Hz, 2H), 8.88 (s, 2H), 8.14 (dd, J = 5.85, 1.2 Hz, 2H), 1.72 (s, 15H). ^{13}C{^{1}H} NMR (75 MHz, CD_3CN): δ(ppm) 154.7, 153.6, 140.9 (q, $^1J_{C,F}$ = 35.6 Hz, CF_3), 124.8 (q, $^4J_{C,F}$ = 3.75 Hz), 123.9, 121.1 (q, $^4J_{C,F}$ = 3.75 Hz), 98.2 (d, $^1J_{C,Rh}$ = 8.25 Hz), 8.27. ^{19}F NMR (CD_3CN): δ(ppm) −65.39. ESI-MS(+) (CH_3OH): *m*/*Z* calcd for $C_{22}H_{21}ClF_6N_2Rh$ 565.04, found 565.1 (M^+). FT-IR (CD_3CN): ν_{max} (cm^{-1}) 3630, 3542, 2104, 1632, 1412, 1344, 1326, 1292, 1275, 1186, 1156. *Anal.* Calcd. for $C_{22}H_{21}N_2Cl_2F_6Rh$ (601.22): C 43.95, H 3.52, N 4.66; Found: C 43.90, H 3.49, N 4.69.

Electrochemistry. All cyclic voltammetry (CVs) experiments were performed in a conventional three-electrode two-compartment cell, using the potentiostat SP 300 Bio-Logic (Bio-Logic Science Instruments SAS). Glassy carbon electrode (GCE, 1mm diameter) was used as working electrode and was polished using a 1 µm diamond suspension and 0.05 µm alumina slurry. A silver wire was used as the reference electrode, and all potential values are reported versus the potential of the $Fc^{+/0}$ couple that was added as an internal standard to the solution after the measurements. A platinum counter electrode was placed in a separate compartment connected to the main compartment by a glass-frit and filled with the supporting electrolyte solution. Studied complexes were dissolved in acetonitrile containing 0.1 M of tetrabutylammonium hexafluorophosphate ($TBAPF_6$, Sigma-Aldrich) as the supporting electrolyte and were bubbled with Ar for 30 minutes before measuring CVs.

Photochemical assays. Photochemical reactions were performed using a 300 W, high pressure Xe arc lamp (Oriel Instruments). The beam was passed through an infrared filter, a collimating lens, a filter holder equipped with a 415 nm band pass filter. Samples were prepared in a 1 cm path length quartz cuvette (Starna) which was placed in a temperature controlled cuvette holder (Quantum Northwest) maintained at 20°C with a circulated water bath. The solvent consists of a CO_2-saturated mixture of acetonitrile (CH_3CN) and triethanolamine (TEOA) in 5:1 volumetric ratio, in which TEOA acts as both a sacrificial electron donor and a source of protons. 1.0 mM of $[Ru(bpy)_3]Cl_2$ was used as a photosensitizer, which is in a 10-fold excess with respect to the $[Rh(R\text{-}bpy)(Cp^*)Cl]^+$ catalyst. Samples were saturated with CO_2 via directly bubbling CO_2 through the solution mixture for 10 minutes.

Product detection. H_2 measurements were performed by gas chromatography on a Shimadzu GC-2014 equipped with a Quadrex column, a Thermal Conductivity Detector with N_2 as a carrier gas. CO was measured using a Shimadzu GC-2010 Plus gas chromatography, fitted with a S9 Restek Shin Carbon column, Helium carrier gas, a methanizer and a Flame Ionization Detector. The typical volume of gas injected was 50 µL.

Formate concentration was determined using a Metrohm 883 Basic IC plus ionic exchange chromatography instrument, using a Metrosep A Supp 5 column and a conductivity detector. A typical measurement requires the sampling of 200 µL of solution (except in kinetic studies where 15 µL aliquots were sampled), followed by a 100 times dilution in deionised 18 MΩ water and injection of 20 µL into the instrument.

Computational Details. All molecular geometries were fully optimized at the M11-L[69]/def2-TZVP level of density functional theory (DFT) using the Gaussian 09 software package[70] and the SMD implicit-solvation model (ε = 35.688 for acetonitrile).[31] Quasi-relativistic LANL2TZ(f) pseudopotential was used for Rh.[32,73] The integral evaluation made use of the grid defined as "ultrafine" in G09. Harmonic vibrational frequencies were computed on the optimized geometries to ensure that all local minima display real frequencies only, whereas the transition states were characterized by a single imaginary frequency. Thermochemical contributions were calculated using the ideal gas, rigid rotor, and harmonic oscillator approximations at a temperature of 298.15 K. The activation barriers were computed using Et_3NH^+ as an explicit proton source.

ASSOCIATED CONTENT

Supporting Information. Supporting electrochemical data (Figures S1-S2), photochemical experiments (Figures S3-S9), FT-IR

spectra (S10-S17), computational details and Cartesian coordinates of all the species involved. This material is available free of charge via the Internet at http://pubs.acs.org.

AUTHOR INFORMATION

Corresponding Author

*E-mail for M.F.: marc.fontecave@college-de-france.fr

ORCID

Tanya K. Todorova: 0000-0002-7731-6498
Hemlata Agarwala: 0000-0001-7347-3093
Marc Fontecave: 0000-0002-8016-4747

Author Contributions

The manuscript was written through contributions of all authors.

Notes

The authors declare no competing financial interest.

ACKNOWLEDGMENT

We acknowledge support by the French State Program 'Investissements d'Avenir' (Grants "LABEX DYNAMO", ANR-11-LABX-0011) and French National Research Agency (ANR, PhotoCarb ANR-16-CE05-0025-01). T.K.T. is grateful to David Wakerley for insightful discussions and X.W. thanks Matthew B. Chambers for the help in setting up the photochemical experiments. The calculations were performed using the HPC resources of GENCI (TGCC) through Grant 2018-810082.

REFERENCES

(1) Arakawa, H.; Aresta, M.; Armor, J. N.; Barteau, M. A.; Beckman, E. J.; Bell, A. T.; Bercaw, J. E.; Creutz, C.; Dinjus, E.; Dixon, D. A.; et al. Catalysis Research of Relevance to Carbon Management: Progress, Challenges, and Opportunities. *Chem. Rev.* **2001**, *101* (4), 953–996.

(2) Benson, E. E.; Kubiak, C. P.; Sathrum, A. J.; Smieja, J. M. Electrocatalytic and Homogeneous Approaches to Conversion of CO2 to Liquid Fuels. *Chem. Soc. Rev.* **2008**, *38* (1), 89–99.

(3) Mikkelsen, M.; Jørgensen, M.; Krebs, F. C. The Teraton Challenge. A Review of Fixation and Transformation of Carbon Dioxide. *Energy Environ. Sci.* **2010**, *3* (1), 43–81.

(4) Appel, A. M.; Bercaw, J. E.; Bocarsly, A. B.; Dobbek, H.; DuBois, D. L.; Dupuis, M.; Ferry, J. G.; Fujita, E.; Hille, R.; Kenis, P. J. A.; et al. Frontiers, Opportunities, and Challenges in Biochemical and Chemical Catalysis of CO2 Fixation. *Chem. Rev.* **2013**, *113* (8), 6621–6658.

(5) Senftle, T. P.; Carter, E. A. The Holy Grail: Chemistry Enabling an Economically Viable CO2 Capture, Utilization, and Storage Strategy. *Acc. Chem. Res.* **2017**, *50* (3), 472–475.

(6) Rakowski Dubois, M.; Dubois, D. L. Development of Molecular Electrocatalysts for CO2 Reduction and H2 Production/Oxidation. *Acc. Chem. Res.* **2009**, *42* (12), 1974–1982.

(7) Morris, A. J.; Meyer, G. J.; Fujita, E. Molecular Approaches to the Photocatalytic Reduction of Carbon Dioxide for Solar Fuels. *Acc. Chem. Res.* **2009**, *42* (12), 1983–1994. https://doi.org/10.1021/ar9001679.

(8) Costentin, C.; Robert, M.; Savéant, J.-M. Current Issues in Molecular Catalysis Illustrated by Iron Porphyrins as Catalysts of the CO2-to-CO Electrochemical Conversion. *Acc. Chem. Res.* **2015**, *48* (12), 2996–3006.

(9) Chen, L.; Guo, Z.; Wei, X.-G.; Gallenkamp, C.; Bonin, J.; Anxolabéhère-Mallart, E.; Lau, K.-C.; Lau, T.-C.; Robert, M. Molecular Catalysis of the Electrochemical and Photochemical Reduction of CO2 with Earth-Abundant Metal Complexes. Selective Production of CO vs HCOOH by Switching of the Metal Center. *J. Am. Chem. Soc.* **2015**, *137* (34), 10918–10921.

(10) Francke, R.; Schille, B.; Roemelt, M. Homogeneously Catalyzed Electroreduction of Carbon Dioxide—Methods, Mechanisms, and Catalysts. *Chem. Rev.* **2018**, *118* (9), 4631–4701.

(11) Costentin, C.; Drouet, S.; Robert, M.; Savéant, J.-M. A Local Proton Source Enhances CO_2 Electroreduction to CO by a Molecular Fe Catalyst. *Science* **2012**, *338* (6103), 90–94.

(12) Costentin, C.; Robert, M.; Savéant, J.-M. Catalysis of the Electrochemical Reduction of Carbon Dioxide. *Chem. Soc. Rev.* **2013**, *42* (6), 2423–2436.

(13) Smieja, J. M.; Sampson, M. D.; Grice, K. A.; Benson, E. E.; Froehlich, J. D.; Kubiak, C. P. Manganese as a Substitute for Rhenium in CO2 Reduction Catalysts: The Importance of Acids. *Inorg. Chem.* **2013**, *52* (5), 2484–2491.

(14) Sampson, M. D.; Nguyen, A. D.; Grice, K. A.; Moore, C. E.; Rheingold, A. L.; Kubiak, C. P. Manganese Catalysts with Bulky Bipyridine Ligands for the Electrocatalytic Reduction of Carbon Dioxide: Eliminating Dimerization and Altering Catalysis. *J. Am. Chem. Soc.* **2014**, *136* (14), 5460–5471.

(15) Machan, C. W.; Stanton, C. J.; Vandezande, J. E.; Majetich, G. F.; Schaefer, H. F.; Kubiak, C. P.; Agarwal, J. Electrocatalytic Reduction of Carbon Dioxide by Mn(CN)(2,2′-bipyridine)(CO)3: CN Coordination Alters Mechanism. *Inorg. Chem.* **2015**, *54* (17), 8849–8856.

(16) Ngo, K. T.; McKinnon, M.; Mahanti, B.; Narayanan, R.; Grills, D. C.; Ertem, M. Z.; Rochford, J. Turning on the Protonation-First Pathway for Electrocatalytic CO2 Reduction by Manganese Bipyridyl Tricarbonyl Complexes. *J. Am. Chem. Soc.* **2017**, *139* (7), 2604–2618.

(17) Franco, F.; Cometto, C.; Nencini, L.; Barolo, C.; Sordello, F.; Minero, C.; Fiedler, J.; Robert, M.; Gobetto, R.; Nervi, C. Local Proton Source in Electrocatalytic CO2 Reduction with [Mn(bpy–R)(CO)3Br] Complexes. *Chem. – Eur. J.* **2017**, *23* (20), 4782–4793.

(18) Elgrishi, N.; Chambers, M. B.; Fontecave, M. Turning It off! Disfavouring Hydrogen Evolution to Enhance Selectivity for CO Production during Homogeneous CO2 Reduction by Cobalt–terpyridine Complexes. *Chem. Sci.* **2015**, *6* (4), 2522–2531.

(19) White, T. A.; Maji, S.; Ott, S. Mechanistic Insights into Electrocatalytic CO2 Reduction within [RuII(tpy)(NN)X]n+ Architectures. *Dalton Trans.* **2014**, *43* (40), 15028–15037.

(20) Johnson, B. A.; Agarwala, H.; White, T. A.; Mijangos, E.; Maji, S.; Ott, S. Judicious Ligand Design in Ruthenium Polypyridyl CO2 Reduction Catalysts to Enhance Reactivity by Steric and Electronic Effects. *Chem. – Eur. J.* **2016**, *22* (42), 14870–14880.

(21) Johnson, B. A.; Maji, S.; Agarwala, H.; White, T. A.; Mijangos, E.; Ott, S. Activating a Low Overpotential CO2 Reduction Mechanism by a Strategic Ligand Modification on a Ruthenium Polypyridyl Catalyst. *Angew. Chem. Int. Ed.* **2016**, *55* (5), 1825–1829.

(22) Reuillard, B.; Ly, K. H.; Rosser, T. E.; Kuehnel, M. F.; Zebger, I.; Reisner, E. Tuning Product Selectivity for Aqueous CO2 Reduction with a Mn(bipyridine)-Pyrene

Catalyst Immobilized on a Carbon Nanotube Electrode. *J. Am. Chem. Soc.* **2017**, *139* (41), 14425–14435.

(23) Kuehnel, M. F.; Orchard, K. L.; Dalle, K. E.; Reisner, E. Selective Photocatalytic CO2 Reduction in Water through Anchoring of a Molecular Ni Catalyst on CdS Nanocrystals. *J. Am. Chem. Soc.* **2017**, *139* (21), 7217–7223.

(24) Elgrishi, N.; Chambers, M. B.; Wang, X.; Fontecave, M. Molecular Polypyridine-Based Metal Complexes as Catalysts for the Reduction of CO2. *Chem. Soc. Rev.* **2017**.

(25) Azcarate, I.; Costentin, C.; Robert, M.; Savéant, J.-M. Dissection of Electronic Substituent Effects in Multielectron–Multistep Molecular Catalysis. Electrochemical CO2-to-CO Conversion Catalyzed by Iron Porphyrins. *J. Phys. Chem. C* **2016**, *120* (51), 28951–28960.

(26) Ching, H. Y. V.; Wang, X.; He, M.; Perujo Holland, N.; Guillot, R.; Slim, C.; Griveau, S.; Bertrand, H. C.; Policar, C.; Bedioui, F.; et al. Rhenium Complexes Based on 2-Pyridyl-1,2,3-Triazole Ligands: A New Class of CO2 Reduction Catalysts. *Inorg. Chem.* **2017**, *56* (5), 2966–2976.

(27) Clark, M. L.; Cheung, P. L.; Lessio, M.; Carter, E. A.; Kubiak, C. P. Kinetic and Mechanistic Effects of Bipyridine (Bpy) Substituent, Labile Ligand, and Brønsted Acid on Electrocatalytic CO2 Reduction by Re(bpy) Complexes. *ACS Catal.* **2018**, 2021–2029.

(28) DuBois, D. L. Development of Molecular Electrocatalysts for Energy Storage. *Inorg. Chem.* **2014**, *53* (8), 3935–3960.

(29) Azcarate, I.; Costentin, C.; Robert, M.; Savéant, J.-M. Dissection of Electronic Substituent Effects in Multielectron–Multistep Molecular Catalysis. Electrochemical CO2-to-CO Conversion Catalyzed by Iron Porphyrins. *J. Phys. Chem. C* **2016**, *120* (51), 28951–28960.

(30) Roy, S.; Sharma, B.; Pécaut, J.; Simon, P.; Fontecave, M.; Tran, P. D.; Derat, E.; Artero, V. Molecular Cobalt Complexes with Pendant Amines for Selective Electrocatalytic Reduction of Carbon Dioxide to Formic Acid. *J. Am. Chem. Soc.* **2017**, *139* (10), 3685–3696.

(31) Inglis, J. L.; MacLean, B. J.; Pryce, M. T.; Vos, J. G. Electrocatalytic Pathways towards Sustainable Fuel Production from Water and CO2. *Coord. Chem. Rev.* **2012**, *256* (21–22), 2571–2600.

(32) Loewen, N. D.; Thompson, E. J.; Kagan, M.; Banales, C. L.; Myers, T. W.; Fettinger, J. C.; Berben, L. A. A Pendant Proton Shuttle on [Fe4N(CO)12]− Alters Product Selectivity in Formate vs. H2 Production via the Hydride [H–Fe4N(CO)12]−. *Chem. Sci.* **2016**, *7* (4), 2728–2735.

(33) Taheri, A.; Thompson, E. J.; Fettinger, J. C.; Berben, L. A. An Iron Electrocatalyst for Selective Reduction of CO2 to Formate in Water: Including Thermochemical Insights. *ACS Catal.* **2015**, *5* (12), 7140–7151.

(34) Taheri, A.; Berben, L. A. Tailoring Electrocatalysts for Selective CO2 or H+ Reduction: Iron Carbonyl Clusters as a Case Study. *Inorg. Chem.* **2016**, *55* (2), 378–385.

(35) Taheri, A.; Carr, C. R.; Berben, L. A. Electrochemical Methods for Assessing Kinetic Factors in the Reduction of CO2 to Formate: Implications for Improving Electrocatalyst Design. *ACS Catal.* **2018**, 5787–5793.

(36) Ceballos, B. M.; Yang, J. Y. Directing the Reactivity of Metal Hydrides for Selective CO2 Reduction. *Proc. Natl. Acad. Sci.* **2018**, *115* (50), 12686–12691.

(37) Takeda, H.; Cometto, C.; Ishitani, O.; Robert, M. Electrons, Photons, Protons and Earth-Abundant Metal Complexes for Molecular Catalysis of CO2 Reduction. *ACS Catal.* **2016**, 70–88.

(38) Elgrishi, N.; Chambers, M. B.; Wang, X.; Fontecave, M. Molecular Polypyridine-Based Metal Complexes as Catalysts for the Reduction of CO2. *Chem. Soc. Rev.* **2017**, *46* (3), 761–796.

(39) Mengele, A. K.; Rau, S. Product Selectivity in Homogeneous Artificial Photosynthesis Using [(bpy)Rh(Cp*)X]n+-Based Catalysts. *Inorganics* **2017**, *5* (2), 35.

(40) Pitman, C. L.; Finster, O. N. L.; Miller, A. J. M. Cyclopentadiene-Mediated Hydride Transfer from Rhodium Complexes. *Chem. Commun.* **2016**, *52* (58), 9105–9108.

(41) Kölle, U.; Grützel, M. Organometallic Rhodium(III) Complexes as Catalysts for the Photoreduction of Protons to Hydrogen on Colloidal TiO2. *Angew. Chem. Int. Ed. Engl.* **1987**, *26* (6), 567–570.

(42) Cosnier, S.; Deronzier, A.; Vlachopoulos, N. Carbon/poly {pyrrole-[(C5Me5)RhIII(bpy)Cl]+} Modified Electrodes; a Molecularly-Based Material for Hydrogen Evolution (Bpy = 2,2′-Bipyridine). *J. Chem. Soc. Chem. Commun.* **1989**, *0* (17), 1259–1261.

(43) Chardon-Noblat, S.; Cosnier, S.; Deronzier, A.; Vlachopoulos, N. Electrochemical Properties of [(C5Me5)RhIII(L)Cl]+ Complexes (L = 2,2′-Bipyridine or 1,10-Phenanthroline Derivatives) in Solution in Related Polypyrrolic Films. Application to Electrocatalytic Hydrogen Generation. *J. Electroanal. Chem.* **1993**, *352* (1), 213–228.

(44) Caix, C.; Chardon-Noblat, S.; Deronzier, A.; Moutet, J.-C.; Tingry, S. (Pentamethylcyclopentadienyl)(polypyridyl) Rhodium and Iridium Complexes as Electrocatalysts for the Reduction of Protons to Dihydrogen and the Hydrogenation of Organics. *J. Organomet. Chem.* **1997**, *540* (1), 105–111.

(45) Blakemore, J. D.; Gupta, A.; Warren, J. J.; Brunschwig, B. S.; Gray, H. B. Noncovalent Immobilization of Electrocatalysts on Carbon Electrodes for Fuel Production. *J. Am. Chem. Soc.* **2013**, *135* (49), 18288–18291.

(46) Lattimer, J. R. C.; Blakemore, J. D.; Sattler, W.; Gul, S.; Chatterjee, R.; Yachandra, V. K.; Yano, J.; Brunschwig, B. S.; Lewis, N. S.; Gray, H. B. Assembly, Characterization, and Electrochemical Properties of Immobilized Metal Bipyridyl Complexes on silicon(111) Surfaces. *Dalton Trans.* **2014**, *43* (40), 15004–15012.

(47) Quintana, L. M. A.; Johnson, S. I.; Corona, S. L.; Villatoro, W.; Goddard, W. A.; Takase, M. K.; VanderVelde, D. G.; Winkler, J. R.; Gray, H. B.; Blakemore, J. D. Proton–hydride Tautomerism in Hydrogen Evolution Catalysis. *Proc. Natl. Acad. Sci.* **2016**, *113* (23), 6409–6414.

(48) Caix, C.; Chardon-Noblat, S.; Deronzier, A. Electrocatalytic Reduction of CO2 into Formate with [(η5-Me5C5)M(L)Cl]+ Complexes (L = 2,2′-Bipyridine Ligands; M=Rh(III) and Ir(III)). *J. Electroanal. Chem.* **1997**, *434* (1), 163–170.

(49) Chambers, M. B.; Wang, X.; Elgrishi, N.; Hendon, C. H.; Walsh, A.; Bonnefoy, J.; Canivet, J.; Quadrelli, E. A.; Farrusseng, D.; Mellot-Draznieks, C.; et al. Photocatalytic Carbon Dioxide Reduction with Rhodium-Based Catalysts in Solution and Heterogenized within Metal–Organic Frameworks. *ChemSusChem* **2015**, *8* (4), 603–608.

(50) Wang, X.; Wisser, F. M.; Canivet, J.; Fontecave, M.; Mellot- Draznieks, C. Immobilization of a Full Photosystem in the Large-Pore MIL-101 Metal–Organic Frame-

work for CO2 Reduction. *ChemSusChem* **2018**, *11* (18), 3315–3322.

(51) Johnson, S. I.; Gray, H. B.; Blakemore, J. D.; Goddard, W. A. Role of Ligand Protonation in Dihydrogen Evolution from a Pentamethylcyclopentadienyl Rhodium Catalyst. *Inorg. Chem.* **2017**, *56* (18), 11375–11386.

(52) Henke, W. C.; Lionetti, D.; Moore, W. N. G.; Hopkins, J. A.; Day, V. W.; Blakemore, J. D. Ligand Substituents Govern the Efficiency and Mechanistic Path of Hydrogen Production with [Cp*Rh] Catalysts. *ChemSusChem* **2017**, *10* (22), 4589–4598.

(53) Lionetti, D.; Day, V. W.; Blakemore, J. D. Synthesis and Electrochemical Properties of Half-Sandwich Rhodium and Iridium Methyl Complexes. *Organometallics* **2017**, *36* (10), 1897–1905.

(54) Peng, Y.; Ramos-Garcés, M. V.; Lionetti, D.; Blakemore, J. D. Structural and Electrochemical Consequences of [Cp*] Ligand Protonation. *Inorg. Chem.* **2017**, *56* (17), 10824–10831.

(55) Hansch, C.; Leo, A.; Taft, R. W. A Survey of Hammett Substituent Constants and Resonance and Field Parameters. *Chem. Rev.* **1991**, *91* (2), 165–195.

(56) Al-Rawashdeh, N. A. F.; Chatterjee, S.; Krause, J. A.; Connick, W. B. Ruthenium Bis-Diimine Complexes with a Chelating Thioether Ligand: Delineating 1,10-Phenanthrolinyl and 2,2′-Bipyridyl Ligand Substituent Effects. *Inorg. Chem.* **2014**, *53* (1), 294–307.

(57) Aroua, S.; Todorova, T. K.; Hommes, P.; Chamoreau, L.-M.; Reissig, H.-U.; Mougel, V.; Fontecave, M. Synthesis, Characterization, and DFT Analysis of Bis-Terpyridyl-Based Molecular Cobalt Complexes. *Inorg. Chem.* **2017**, *56* (10), 5930–5940.

(58) Ghosh, D.; Takeda, H.; Fabry, D. C.; Tamaki, Y.; Ishitani, O. Supramolecular Photocatalyst with a Rh(III)-Complex Catalyst Unit for CO2 Reduction. *ACS Sustain. Chem. Eng.* **2019**, *7* (2), 2648–2657.

(59) Pellegrin, Y.; Odobel, F. Sacrificial Electron Donor Reagents for Solar Fuel Production. *Comptes Rendus Chim.* **2017**, *20* (3), 283–295.

(60) Kalyanasundaram, K.; Kiwi, J.; Grätzel, M. Hydrogen Evolution from Water by Visible Light, a Homogeneous Three Component Test System for Redox Catalysis. *Helv. Chim. Acta* **1978**, *61* (7), 2720–2730.

(61) DuBois, D. L.; Berning, D. E. Hydricity of Transition-Metal Hydrides and Its Role in CO2 Reduction. *Appl. Organomet. Chem.* **2000**, *14* (12), 860–862.

(62) Tsay, C.; Livesay, B. N.; Ruelas, S.; Yang, J. Y. Solvation Effects on Transition Metal Hydricity. *J. Am. Chem. Soc.* **2015**, *137* (44), 14114–14121.

(63) Mondal, B.; Neese, F.; Ye, S. Control in the Rate-Determining Step Provides a Promising Strategy To Develop New Catalysts for CO2 Hydrogenation: A Local Pair Natural Orbital Coupled Cluster Theory Study. *Inorg. Chem.* **2015**, *54* (15), 7192–7198.

(64) Mondal, B.; Neese, F.; Ye, S. Toward Rational Design of 3d Transition Metal Catalysts for CO2 Hydrogenation Based on Insights into Hydricity-Controlled Rate-Determining Steps. *Inorg. Chem.* **2016**, *55* (11), 5438–5444.

(65) Waldie, K. M.; Ostericher, A. L.; Reineke, M. H.; Sasayama, A. F.; Kubiak, C. P. Hydricity of Transition-Metal Hydrides: Thermodynamic Considerations for CO2 Reduction. *ACS Catal.* **2017**, 1313–1324.

(66) Ellis, W. W.; Miedaner, A.; Curtis, C. J.; Gibson, D. H.; DuBois, D. L. Hydride Donor Abilities and Bond Dissociation Free Energies of Transition Metal Formyl Complexes. *J. Am. Chem. Soc.* **2002**, *124* (9), 1926–1932.

(67) Rawat, K. S.; Mahata, A.; Choudhuri, I.; Pathak, B. Catalytic Hydrogenation of CO2 by Manganese Complexes: Role of π-Acceptor Ligands. *J. Phys. Chem. C* **2016**, *120* (30), 16478–16488.

(68) Rawat, K. S.; Mahata, A.; Pathak, B. Catalytic Hydrogenation of CO2 by Fe Complexes Containing Pendant Amines: Role of Water and Base. *J. Phys. Chem. C* **2016**, *120* (47), 26652–26662.

(69) Peverati, R.; Truhlar, D. G. M11-L: A Local Density Functional That Provides Improved Accuracy for Electronic Structure Calculations in Chemistry and Physics. *J. Phys. Chem. Lett.* **2012**, *3* (1), 117–124.

(70) Frisch, M. J.; Trucks, G. W.; Cheeseman, J. R.; Scalmani, G.; Caricato, M.; Hratchian, H. P.; Li, X.; Barone, V.; Bloino, J.; Zheng, G.; et al. *Gaussian 09*; Gaussian, Inc.: Wallington CT., 2013.

(71) Marenich, A. V.; Cramer, C. J.; Truhlar, D. G. Universal Solvation Model Based on Solute Electron Density and on a Continuum Model of the Solvent Defined by the Bulk Dielectric Constant and Atomic Surface Tensions. *J. Phys. Chem. B* **2009**, *113* (18), 6378–6396.

(72) Ehlers, A. W.; Böhme, M.; Dapprich, S.; Gobbi, A.; Höllwarth, A.; Jonas, V.; Köhler, K. F.; Stegmann, R.; Veldkamp, A.; Frenking, G. A Set of F-Polarization Functions for Pseudo-Potential Basis Sets of the Transition Metals Sc-Cu, Y-Ag and La-Au. *Chem. Phys. Lett.* **1993**, *208* (1), 111–114.

(73) Roy, L. E.; Hay, P. J.; Martin, R. L. Revised Basis Sets for the LANL Effective Core Potentials. *J. Chem. Theory Comput.* **2008**, *4* (7), 1029–1031.

Table of Contents (TOC)

Synopsys: We report a photochemical CO_2 reduction study on a series of $[Rh(R\text{-}bpy)(Cp^*)Cl]^+$ complexes and show how modifications in the electronic structure of the catalyst affect its selectivity, defined as the HCOOH : H_2 product ratio. DFT computations were used to explain the observed tendency of electron-donating substituents to favor CO_2 reduction by means of lowering the hydride transfer barrier towards formic acid production, as compared to substituents with electron-withdrawing nature that favor more strongly the proton reduction to hydrogen.